The Capability of Amphibole in Tracing the Physicochemical Processes of Magma Mixing

Mingjian Li[1,2], Yunchuan Zeng[1] , Massimo Tiepolo[2], Jifeng Xu[1] , Enrico Cannaò[2] , Francesca Forni[2] , and Feng Huang[1]

[1]School of Earth Science and Resources, Frontiers Science Center for Deep-time Digital Earth, and State Key Laboratory of Geological Processes and Mineral Resources, China University of Geosciences, Beijing, China, [2]Dipartimento di Scienze della Terra "A. Desio", Università degli Studi di Milano, Milano, Italy

Abstract This study explores the capability of amphibole in tracing the physicochemical process of magma mixing through spatially associated gabbros, mafic microgranular enclaves (MMEs) and granodiorites from central Tibet. These rocks share similar zircon ages as well as zircon Hf-O and plagioclase Sr isotopes. However, the amphiboles within the gabbros and granodiorites have different Sr and B isotope compositions, while amphiboles with both heterogeneous isotopic imprints occur in the MMEs. According to data and modeling, significant mixing of two isotopically distinct magmas is recorded by amphibole but not by zircon and plagioclase. Based on a synthesis of petrography, geochemistry and thermobarometry, we interpret this inconsistency by the crystallization order of minerals and propose that magma mixing occurred after the parent magma was emplaced at ~10 km and cooled to ~750°C. Our study highlights that amphibole may be a more sensitive tracer of magma mixing relative to other commonly used methods.

Plain Language Summary Magma mixing significantly shapes the composition of silicic igneous rocks representing the major constituent of the upper continental crust. Since bulk-rock composition may only bear the average of mixed sources, in situ techniques such as Hf-O isotopes in zircon and Sr-Pb isotopes in plagioclase are widely used to investigate the details of magma mixing. However, these methods cannot constrain how magma mixing operates in the deep crust. This study novelly uses in situ Sr-B isotopes and trace elements in amphibole to trace the physicochemical process of magma mixing through spatially associated gabbros, mafic microgranular enclaves and granodiorites from the central Tibetan Plateau. Our data show that significant mixing of two isotopically distinct magmas is recorded by amphibole but not by zircon and plagioclase. We demonstrate that the amphibole geochemistry (i.e., trace element, Sr-B isotope compositions) may be more sensitive in tracing magma mixing relative to traditional isotopic tools and has the potential to unravel the physicochemical process(es) of magma mixing in the deep crust. In addition, our work reinforces the use of B isotopes in amphibole to discern the nature (fluids released from altered oceanic crust vs. residual slab) of the slab components that metasomatized the supra-subduction mantle.

1. Introduction

Magma mixing significantly shapes the composition of silicic igneous rocks, representing the major constituent of the upper continental crust. Because bulk-rock composition may only bear the average of mixed sources (e.g., Barnes et al., 2021), in situ techniques such as Hf-O isotopes in zircon and Sr isotopes in clinopyroxene and plagioclase are widely used to investigate magma mixing processes (e.g., Francalanci et al., 2005; Kemp et al., 2007). Zircon and plagioclase, however, are unable to provide the physicochemical conditions of melt crystallization (pressure and/or temperature) and thus the record of magma mixing is decoupled from the *P-T* conditions, leaving a key question unanswered: where does magma mixing occur in the crust? Clinopyroxene is a good geo-thermo-barometer but is relatively sparse in felsic igneous rocks. Amphibole, a principal mineral of igneous rocks of wide compositions, is deemed to play a major role in forming felsic igneous rocks (Davidson et al., 2007). Furthermore, amphibole is among the most useful minerals in reconstructing the physicochemical conditions of melt crystallization because of the well-calibrated thermobarometers and amphibole-melt trace element partition coefficients (Ridolfi et al., 2010; Schmidt, 1992; Tiepolo et al., 2007). So far, O-H and B isotopes in amphibole have been used to investigate metasomatic processes in the mantle (e.g., Banerjee et al., 2018; Cannaò et al., 2022), while little attention has been devoted to the role of amphibole in the formation of granitoids.
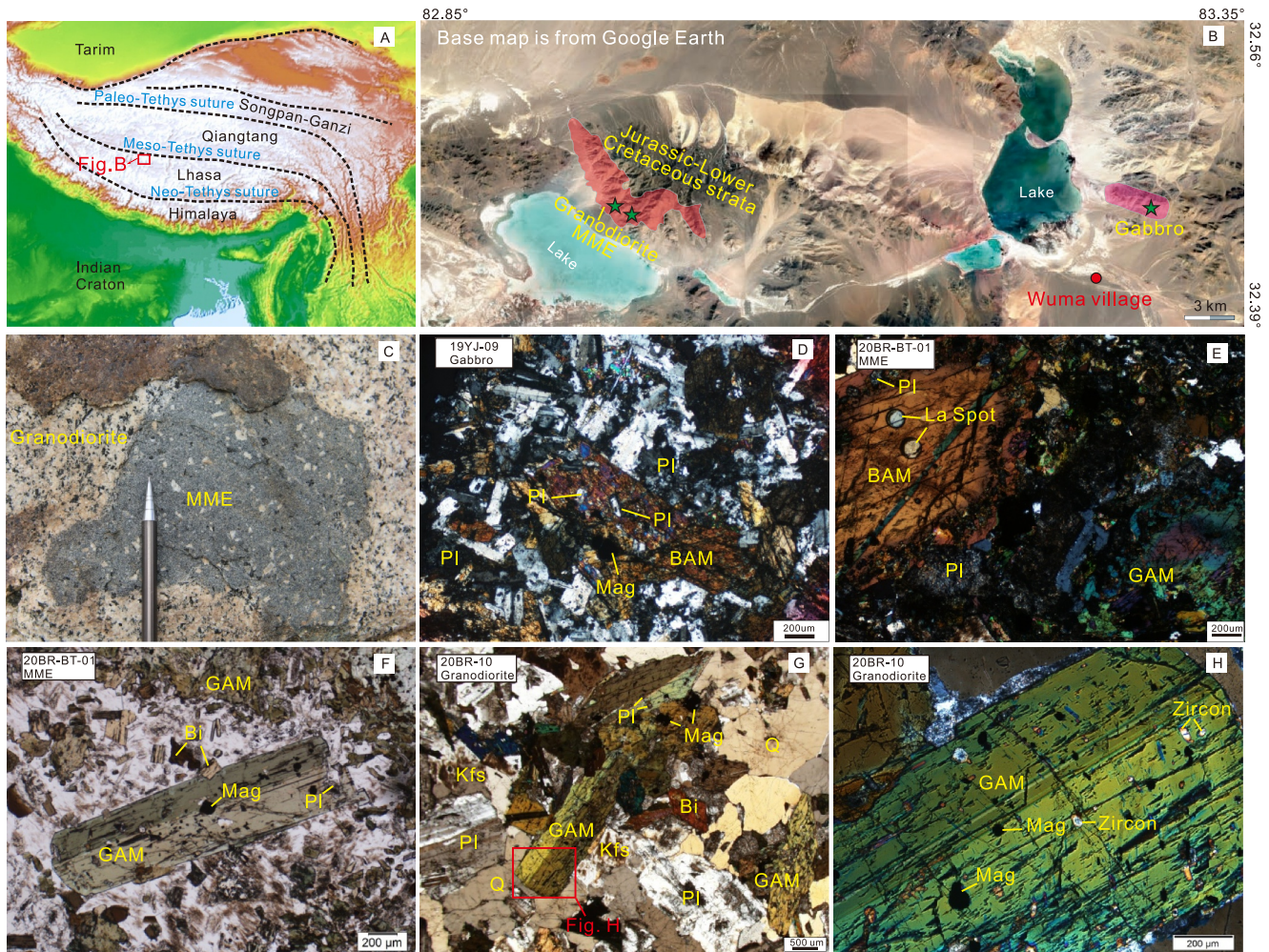
Figure 1. (a) Tectonic framework of Tibetan Plateau; (b) Field distribution of the main lithologies investigated in this work; (c) Field relationship between mafic microgranular enclave and granodiorite; (d)–(h) microphotograph for the Wuma magmatic complex: brown amphiboles are euhedral and contain plagioclase inclusions (d), green amphiboles are mostly subhedral and contain plagioclase and zircon inclusions (f)–(h), whereas K-feldspar is anhedral and grown at the rim of the green amphiboles (g). BAM, brown amphibole; GAM, green amphiboles; Pl, plagioclase; Kfs, K-feldspar; Bi, biotite; Mag, magnetite; Q, quartz.

Here we report bulk-rock and mineral geochemical data on a set of spatially associated gabbros, granodiorites and their hosted mafic microgranular enclaves (MMEs) in central Tibet. Our results shed light on the capability of amphibole geochemistry (trace elements and Sr-B isotopes) in tracing the physicochemical process of deep crustal magma mixing and in discerning the nature (fluids released from altered oceanic crust vs. residual slab) of the slab components that metasomatized supra-subduction mantle.

2. Geological Background and Petrography

The gabbro, granodiorite and their hosted MMEs samples were collected near the Wuma village, and tectonically belong to the northern Lhasa Block of Tibetan Plateau (Figures 1a and 1b). These rocks intrude into the Jurassic to Lower Cretaceous sedimentary strata at ca. 110 Ma (Wei et al., 2018). Early Cretaceous magmatic rocks are widespread on the northern Lhasa Block (Figure S1 in Supporting Information S1), most of which are granitoids with depleted Sr-Hf-Nd isotopic compositions and thereby imply a juvenile lower crust underneath (Zeng et al., 2020; Zhu et al., 2011). Three competing hypotheses have been proposed to explain the tectonic setting responsible for the formation of these rocks, including post-collision lithospheric delamination following the Lhasa-Qiangtang continental collision (Hu et al., 2017), southward subduction of Meso-Tethyan lithosphere (Zhu et al., 2011), or northward subduction of the Neo-Tethyan lithosphere (Figure S1 in Supporting Information S1; Kapp & DeCelles, 2019; M. J. Li et al., 2023).
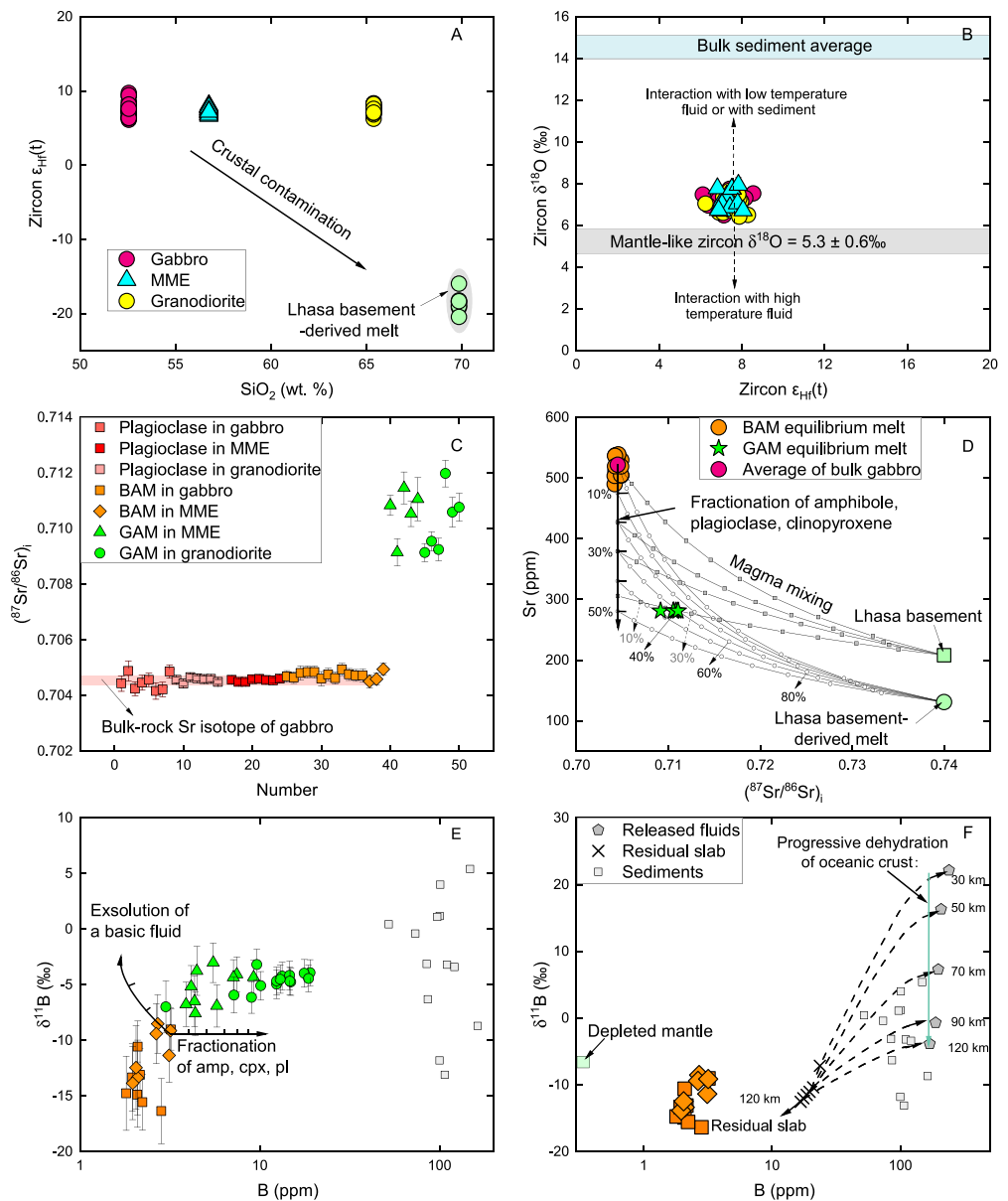
Figure 2. Diagrams of in situ isotope values for zircon ((a) SiO_2 vs. $\varepsilon_{Hf}(t)$—(b) $\varepsilon_{Hf}(t)$ vs. $\delta^{18}O$), plagioclase and amphibole ((c) $^{87}Sr/^{86}Sr$—(e) B vs. $\delta^{11}B$) from the gabbros, mafic microgranular enclaves and granodiorite in the northern Lhasa Block. In (a)–(b), the Sr and Hf isotopes of Lhasa basement-derived melt are represented by the Jurassic S-type granite (Zhu et al., 2011), and the O isotope of bulk sediment average is from Spencer et al. (2014). In (d), the parameters used for magma mixing between mean gabbro composition and basement (bulk-rock) or their melt in the $^{87}Sr/^{86}Sr$ versus Sr diagram are present in Table S12 of Supporting Information S1. In (f), the calculated $\delta^{11}B$ and B contents for slab-derived fluids and complementary residual slab during progressive dehydration (from 30 to 120 km) are based on Tonarini et al. (2011). BAM, brown amphibole; GAM, green amphiboles.

The mineral assemblages of the three rock types are summarized in Table S1 of Supporting Information S1 and representatively shown by photomicrographs in Figure 1. In brief, amphibole and plagioclase are the dominant minerals among the three rock types, while K-feldspar, biotite and quartz are only present in the MMEs and granodiorite. Accessory minerals in the three types of rocks are similar, which are zircon, apatite, and magnetite. Notably, the amphiboles in the MME occur either as brown or green grain (Figures 2e and 2f), reflecting different chemical compositions (Table S2 in Supporting Information S1), while the gabbros only contain brown amphiboles.

3. Analytical Results

Representative samples were analyzed for zircon U-Pb geochronology and Lu-Hf isotope, bulk-rock element and Sr-Nd isotope, and in situ mineral element and Sr-B isotope compositions (analytical methods and data are present in the Text and Tables S2–S11 in Supporting Information S1). U-Pb zircon geochronology yields mean age of 110.3 ± 1.1 Ma (1σ) for the gabbro, 113.6 ± 0.6 Ma (1σ) for the MME, and 113.1 ± 0.6 Ma (1σ) for granodiorite (Figure S2 in Supporting Information S1). However, the $^{206}Pb/^{238}U$ age of individual zircon grains in the gabbro (108.1 ± 0.7 Ma to 113.8 ± 1.1 Ma; 1σ), MME (110.3 ± 1.1 Ma to 115.9 ± 1.6 Ma; 1σ), and granodiorite (112.3 ± 1.5 Ma to 114.5 ± 1.5 Ma; 1σ) are broadly overlap. Thus, given the external uncertainty of Laser Ablation Inductively Coupled Plasma Mass Spectrometry zircon U-Pb dating ($\geq 2\%$ at 1σ level; X. Li et al., 2015), we suggest three groups of rocks share similar formation ages within allowed errors and emplaced at ca. 110 Ma. Among the studied rocks, the gabbros have the highest MgO, lowest SiO_2, and most depleted bulk-rock Sr-Nd isotopes ($^{87}Sr/^{86}Sr_i$ = 0.7043 to 0.7044; $\varepsilon_{Nd(t)}$ = +2.36 to +2.41), while the granodiorites have the lowest MgO, highest SiO_2 and most enriched bulk-rock Sr-Nd isotopes ($^{87}Sr/^{86}Sr_i$ = 0.7062 to 0.7072; $\varepsilon_{Nd(t)}$ = +1.27 to +1.58) (Figure S3 and Table S7 in Supporting Information S1). As shown in Figures 2a and 2b, the three rock types have similar and relatively uniform zircon Hf-O isotopic signatures ($\varepsilon_{Hf}(t)$ = +6.1 to +9.7; $\delta^{18}O$ = +6.4 to +7.9‰). Despite the different bulk-rock Sr-Nd isotopic compositions, plagioclases in the three rock types have similar and relatively homogenous Sr isotopic compositions ($^{87}Sr/^{86}Sr$ = 0.7042 to 0.7049; Figure 2c). Furthermore, the major element compositions of plagioclases in the three rock types are similar, with the anorthite component ranging from An_{40} to An_{59} (Figure S4 in Supporting Information S1). In contrast, the Sr and B isotopic ratios of amphiboles in the three rock types have a bimodal distribution and the two clusters mainly reflect amphibole geochemistry. Specifically, according to the Leake et al. (1997) classification scheme, the green amphiboles are magnesiohornblende, while the brown amphiboles are pargasite and edenite. Besides, the green amphiboles exhibit lower Al_2O_3 and TiO_2 contents and more pronounced Zr, Ba, Sr, and Eu negative anomalies compared to brown amphibole (Figures 3a and 3b). Isotopically, brown amphiboles have lower $^{87}Sr/^{86}Sr$ ($^{87}Sr/^{86}Sr$ = 0.7046 to 0.7049) and $\delta^{11}B$ (-16.4 to $-9.0‰$) than the green amphiboles ($^{87}Sr/^{86}Sr$ = 0.7091 to 0.7120; $\delta^{11}B$ = -7.0 to $-3.2‰$) (Figures 2c and 2e). Notably, the in situ Sr isotopic signatures of plagioclase and brown amphibole are similar to that of the bulk gabbro (Figure 2c).

4. Physical Condition of Mineral Crystallization

In amphibole, Al-tschermak substitution is sensitive to variations in pressure whereas Ti-Tschermak variation may reflect changes in pressure, water activity, and temperature, or a combination thereof (Ridolfi et al., 2010; Schmidt, 1992). Thus, the different Al_2O_3 and TiO_2 contents of the green amphiboles and brown amphiboles imply they crystallized under different temperatures and pressures. We use the experimentally calibrated Al-in-hornblende barometer (Schmidt, 1992) and the empirical formulations of thermometer based on a synthesis of experimental results (Ridolfi et al., 2010) to estimate the crystallization pressure and temperature of the melt in equilibrium with the studied amphiboles (Table S2 in Supporting Information S1). Our data reveal that the parental magma of brown amphiboles was hotter (T = 900–960°C; mean = 930°C) and deeper (P = 470–580 Mpa) compared to that of green amphiboles (T = 730–830°C, mean = 770°C; P = 110–390 Mpa; Figures 3c and 3d). Besides, we also estimate the temperatures of zircon crystallization by using the updated Ti-in-zircon thermometer (Loucks et al., 2020), achieving comparable results among the three rock types (T = 760–880°C, mean = 820°C; Table S3 in Supporting Information S1 and Figure 3c).

5. The Apparent Isotope Paradox and Interpretation

The similarities of U-Pb age, Hf-O isotopes and crystallization temperatures for zircon, as well as the Sr isotopic signature of plagioclase, among the nearby three rock types, suggests that zircon and plagioclase crystallized from the same magma plumbing system. In the traditional view, the uniform zircon Hf-O and plagioclase Sr isotopes of the three rock types provide evidence for an isotopically depleted magma source with negligible contribution from isotopically enriched materials (Francalanci et al., 2005; Kemp et al., 2007). However, the in situ Sr isotope data of brown amphiboles and green amphiboles document that the granodiorites and MMEs are the composite of two isotopically distinct end members (i.e., depleted vs. enriched). This apparent isotope paradox can be accounted for by the crystallization order of these minerals. The green amphiboles in the granodiorite and MMEs contain plagioclase and zircon inclusions (Figures 1f–1h) and display pronounced negative Sr, Ba and Zr anomalies (Figure 3b). This, together with the relatively low crystallization temperature of green amphiboles
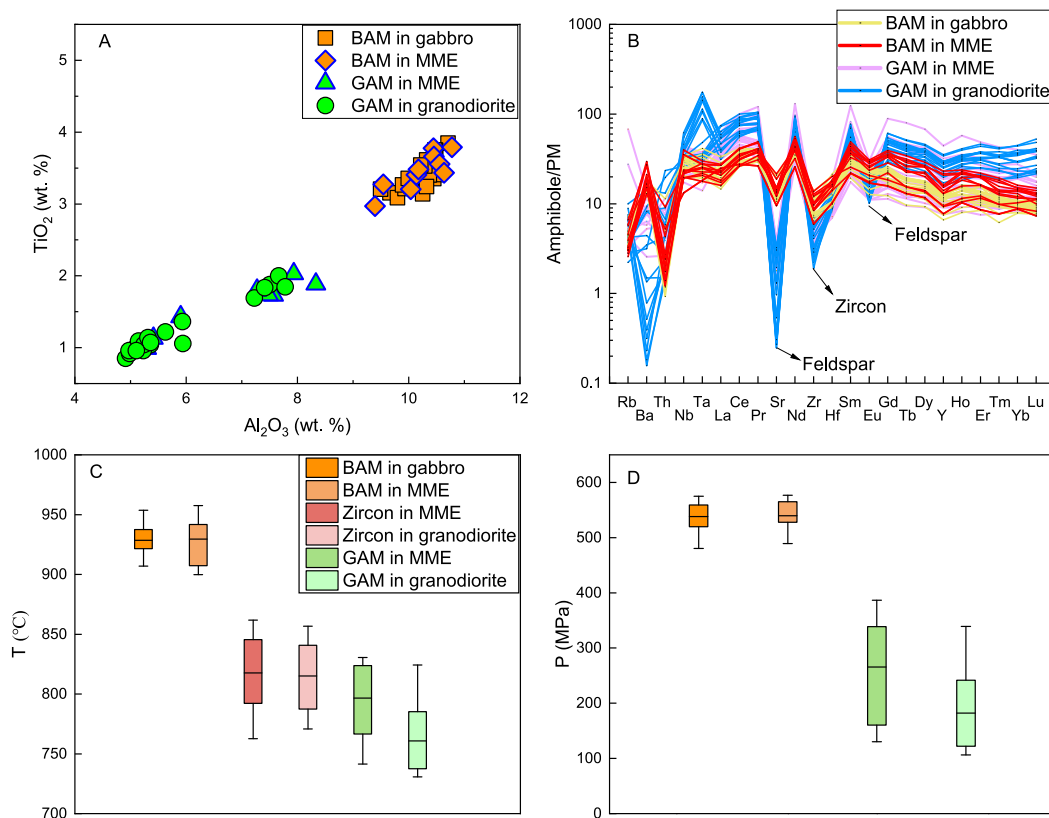
Figure 3. (a) Plot of TiO$_2$ versus Al$_2$O$_3$, (b) trace element distributions, (c) crystallization temperature, and (d) pressure (data in Table S2 of Supporting Information S1) for amphiboles in the Wuma magmatic complex. In (b) the negative anomalies in Zr, Sr, Eu, and Ba reflect zircon, feldspar and biotite crystallization effects. BAM, brown amphibole; GAM, green amphiboles.

(Figure 3c), suggests that they likely crystallized after plagioclase and zircon. The biotites and K-feldspars are the latest crystallized phases as they are mostly anhedral and grow on the rim of the green amphiboles (Figure 1g). K-feldspars likely crystallized after biotites given their pronounced negative Ba anomalies (Figure 3b). In the gabbro, the brown amphiboles are euhedral with plagioclase inclusions (Figure 1d) and display weak or no negative Eu anomalies (Figure 3b), suggesting they crystallized simultaneously with plagioclase. Coupled with the higher crystallization temperature of brown amphibole relative to zircon, we infer that the crystallization sequence is plagioclase ≥ brown amphibole > zircon > green amphibole > biotite > K-feldspar (Table S1 in Supporting Information S1). Thus, the plagioclase, brown amphibole and zircon were most likely crystallized from the uncontaminated magmas having depleted Sr and Hf isotopes. In comparison, green amphiboles (and the minerals crystallized after them like K-feldspar and biotite) in the MMEs and granodiorite likely crystallized from a more evolved magma contaminated by ancient crustal materials, as testified by their more radiogenic Sr isotopic imprints (up to 0.712, Figure 2c, Table S9 in Supporting Information S1).

6. The Physicochemical Framework of Magma Mixing in the Deep Crust

The gabbro lacks cumulate texture (Figure 1d) and geochemical indicators typical of cumulate rocks, such as positive Eu anomalies for plagioclase cumulation, and convex upward chondrite-normalized rare earth element (REE) abundance patterns for amphibole cumulation (Figure S3d in Supporting Information S1), which, there-fore, likely represent solid magmas. The lower MgO and the higher SiO$_2$ contents of the granodiorite compared to the MMEs are likely due to fractional crystallization processes rather than to different degrees of crustal assimilation since the green amphiboles in these rocks have similar Sr isotopic imprints (Figure 2c). The brown amphiboles consist only a small proportion of the MME (5%–10%; Table S1 in Supporting Information S1), which may have been completely removed during the magmatic evolution as they are absent in the granodiorite. It
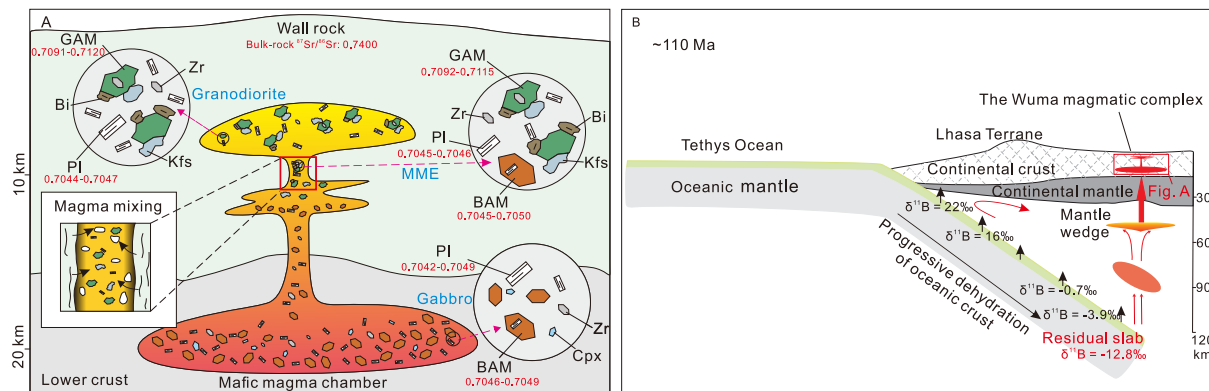
Figure 4. (a) Cartoon illustrating the proposed scenario for the formation of the Wuma magmatic complex. (b) Cartoon illustrating the $\delta^{11}B$ variation along the subducted oceanic slab due to its progressive dehydration and release of B and ^{11}B through Rayleigh fractionation. This process produces residual slab components with extremely low $\delta^{11}B$ values that impact the geochemistry of primitive magma in subduction zones. BAM, brown amphibole; GAM, green amphiboles; Pl, plagioclase; Bi, biotite; Kfs, K-feldspar; Zr, zircon; Cpx, clinopyroxene.

is not uncommon that early-crystallized high-temperature and high-pressure amphiboles are completely removed during evolution of mafic magmas to intermediate-felsic magmas (Davidson et al., 2007; Smith, 2014). The key for the interpretation of magma mixing processes thus is to clarify the origin of the MMEs. The bulk-rock composition of MMEs represents the average of the composite of minerals (and possible intergranular melt) crystallized from the uncontaminated and contaminated magmas and, therefore, they show hybrid composition. For this reason, we calculate the melt composition in equilibrium with the green amphiboles to constrain the composition of the contaminated magma at the beginning. Our modeling indicates that the pristine mafic magmas should have undergone 30%–45% crystallization of an assemblage comprising brown amphibole, plagioclase, and clinopyroxene in the middle-lower (~20 km) part of continental crust (Figures 2d and 4a). Then the residual melts were contaminated by a significant amount (up to 40%) of ancient crustal components to crystallize green amphiboles, K-feldspar and biotite when ascent to ca. 10 km below the surface and cooled down to ca. 750°C (Figures 2d and 4a). Of note, the Zr content in the equilibrium melt of GAMs is relatively low as indicated by their pronounced negative Zr anomalies (Figure 3d), which may restrain crystallization of zircons with enriched Hf isotopes signifying magma contamination.

7. Petrological Implications of Amphibole B Isotope Data

The gabbros are representative of nearly primitive mantle melts given their high MgO (4.5–14.5 wt. %) and Mg# (52–74) (Table S6 in Supporting Information S1). In these rocks, brown amphiboles represent the early-crystallized phase and their $\delta^{11}B$ values are thus reflective of their mantle source. Notably, most brown amphiboles possess lower $\delta^{11}B$ values (−16.4 to −9.0‰) than those of the depleted mantle (*ca.* −7.1‰, Marschall et al., 2017) and of the mafic arc rocks derived from the mantle metasomatized by slab-derived fluid (up to +18‰). This suggests the involvement of a residual (substantially dehydrated) slab component in the mantle source of the studied gabbros (e.g., Kaliwoda et al., 2011; Marschall et al., 2017; Tonarini et al., 2011). Given the unradiogenic Sr isotopes in the brown amphiboles, the slab component responsible for their low $\delta^{11}B$ signature should be derived from a deeply subducted oceanic slab instead of a subducted continental crust. From this perspective, the Early Cretaceous magmatism in the northern Lhasa Block is more likely triggered by subduction of the Neo-Tethyan or Meso-Tethyan slab rather than by lithospheric delamination following the Lhasa-Qiangtang collision (Figure 4b; Zeng et al., 2020; Zhu et al., 2011). Indeed, the B isotopic signatures of amphibole from mafic rocks are not sensitive to magmatic differentiation (i.e., crystal fractionation and magma mixing) being a relatively early-crystallized mineral in hydrous magma. Thus, amphibole has the potential to discern the nature of the slab components that metasomatized supra-subduction mantle regions in other localities. Unfortunately, to date, the B isotope data of amphibole have been rarely investigated (Cannaò et al., 2022; Kaliwoda et al., 2011; Wang et al., 2020), and more studies focusing on the B isotope fractionation between silicate mineral and melt/fluid are needed (e.g., Kowalski & Wunder, 2018).

The $\delta^{11}B$ amphibole-melt fractionation during amphibole crystallization is negligible (Kaliwoda et al., 2011), indicating that the $\delta^{11}B$ of the equilibrium melt should be equal to that of the amphibole. Furthermore, plagioclase crystallizes slightly earlier or simultaneously with brown amphibole, while zircon crystallizes after brown amphibole, both of which B is strongly incompatible (Bindeman & Davis, 2000; Chakraborty et al., 1993; Chowdhury et al., 2020) and their crystallization should thus have limited impact on the $\delta^{11}B$ values of the residual melts. Therefore, the higher $\delta^{11}B$ values in the green amphiboles relative to the brown amphiboles are unlikely related to Rayleigh fractionation, but they are instead proxies of the addition of ^{11}B-rich materials (Figure 2f). Such high $\delta^{11}B$ component may reflect the $\delta^{11}B$ isotopic composition of the assimilant (Palmer & Swihart, 1996) or the fluids released during crustal assimilation (e.g., Kaliwoda et al., 2011). This process is not recorded by the $\delta^{18}O$ of zircons that are widely considered to be sensitive to fluid-rock interaction and/or sediment input (Spencer et al., 2014; Valley et al., 2005; Figure 2b), further bolstering our scenario invoking zircons crystallization before green amphiboles.

8. Conclusions and Outlook

Based on the detailed petrographic and geochemical investigations on the coeval gabbro, MMEs and granodiorite exposed nearby in the northern Lhasa Block, our study highlights that the amphibole geochemistry (i.e., trace element, Sr-B isotope compositions) may be more sensitive in tracing magma mixing relative to traditional isotopic tools such as the Hf and O in zircon and $^{87}Sr/^{86}Sr$ ratios in plagioclase. This is mainly due to the wider range of temperature and pressure stability of amphibole during the ascending of the parental melt, allowing us to unravel the physicochemical process(es) of magma mixing in the deep crust. The role of magma mixing in the formation of granitoid rocks (at least for some like the MMEs and granodiorites in this study) may be considerably underrated by the commonly used isotopic tools. In addition, our work reinforces the use of B isotopes in amphibole to investigate the nature of slab contribution in the genesis of magmatic rocks at subduction zones.

Data Availability Statement

The supplementary tables include data of the assemblage, texture and geochemistry of minerals (Table S1 in Supporting Information S1), in situ amphibole major element compositions (Table S2 in Supporting Information S1), crystallization temperature of the zircon (Table S3 in Supporting Information S1), zircon U-Pb ages and Lu-Hf-O isotope compositions (Tables S4 and S5 in Supporting Information S1), bulk-rock major and trace element compositions (Table S6 in Supporting Information S1), bulk-rock Sr-Nd isotope compositions (Table S7 in Supporting Information S1), in situ amphibole trace element compositions (Table S8 in Supporting Information S1), in situ mineral Sr isotope compositions (Table S9 in Supporting Information S1), in situ amphibole B isotope compositions (Table S10 in Supporting Information S1), in situ plagioclase major element compositions (Table S11 in Supporting Information S1), partition coefficients and end member used for magma fractionation and mixing modeling (Table S12 in Supporting Information S1). The supplementary figures consist of simplified geological map showing the space distributions of Early Cretaceous magmatic rocks (Figure S1 in Supporting Information S1), zircon concordant U–Pb age (Figure S2 in Supporting Information S1), plots of $Na_2O + K_2O$, MgO with SiO_2, $\varepsilon_{Nd}(t)$ versus $(^{87}Sr/^{86}Sr)_i$, and chondrite-normalized rare earth element (Figure S3 in Supporting Information S1), and compositions of plagioclase and amphibole (Figure S4 in Supporting Information S1). All these data can also be found online (M. J. Li et al., 2024).

References

Banerjee, S., Kyser, T. K., & Mitchell, R. H. (2018). Oxygen and hydrogen isotopic composition of phlogopites and amphiboles in diamond-bearing kimberlite hosted MARID xenoliths: Constraints on fluid-rock interaction and recycled crustal material in the deep continental lithospheric mantle. *Chemical Geology*, *479*, 272–285. https://doi.org/10.1016/j.chemgeo.2018.01.022

Barnes, C. G., Werts, K., Memeti, V., Paterson, S. R., & Bremer, R. (2021). A tale of five enclaves: Mineral perspectives on origins of mafic enclaves in the Tuolumne Intrusive Complex. *Geosphere*, *17*(2), 352–374. https://doi.org/10.1130/ges02233.1

Bindeman, I. N., & Davis, A. M. (2000). Trace element partitioning between plagioclase and melt: Investigation of dopant influence on partition behavior. *Geochimica et Cosmochimica Acta*, *64*(16), 2863–2878. https://doi.org/10.1016/s0016-7037(00)00389-6

Cannaò, E., Tiepolo, M., Fumagalli, P., Grieco, G., & Agostini, S. (2022). Metasomatism in the Finero Phlogopite Peridotite: New insights from C and N concentrations and $\delta^{13}C$-$\delta^{11}B$ signatures. *Chemical Geology*, *614*, 121181. https://doi.org/10.1016/j.chemgeo.2022.121181

Chakraborty, S., Dingwell, D. B., & Chaussidon, M. (1993). Chemical diffusivity of boron in melts of haplogranitic composition. *Geochimica et Cosmochimica Acta*, *57*(8), 1741–1751. https://doi.org/10.1016/0016-7037(93)90110-i

Chowdhury, W., Trail, D., & Bell, E. (2020). Boron partitioning between zircon and melt: Insights into Hadean, modern arc, and pegmatitic settings. *Chemical Geology*, *551*, 119763. https://doi.org/10.1016/j.chemgeo.2020.119763

Davidson, J., Turner, S., Handley, H., Macpherson, C., & Dosseto, A. (2007). Amphibole "sponge" in arc crust? *Geology*, *35*(9), 787–790. https://doi.org/10.1130/g23637a.1

Francalanci, L., Davies, G. R., Lustenhouwer, W., Tommasini, S., Mason, P. D., & Conticelli, S. (2005). Intra-grain Sr isotope evidence for crystal recycling and multiple magma reservoirs in the recent activity of Stromboli volcano, southern Italy. *Journal of Petrology*, *46*(10), 1997–2021. https://doi.org/10.1093/petrology/egi045

Hu, P. Y., Zhai, Q. G., Jahn, B. M., Wang, J., Li, C., Chung, S. L., et al. (2017). Late Early Cretaceous magmatic rocks (118–113 Ma) in the middle segment of the Bangong–Nujiang suture zone, Tibetan Plateau: Evidence of lithospheric delamination. *Gondwana Research*, *44*, 116–138. https://doi.org/10.1016/j.gr.2016.12.005

Kaliwoda, M., Marschall, H. R., Marks, M. A., Ludwig, T., Altherr, R., & Markl, G. (2011). Boron and boron isotope systematics in the per-alkaline Ilímaussaq intrusion (South Greenland) and its granitic country rocks: A record of magmatic and hydrothermal processes. *Lithos*, *125*(1–2), 51–64. https://doi.org/10.1016/j.lithos.2011.01.006

Kapp, P., & DeCelles, P. G. (2019). Mesozoic–Cenozoic geological evolution of the Himalayan-Tibetan orogen and working tectonic hypotheses. *American Journal of Science*, *319*(3), 159–254. https://doi.org/10.2475/03.2019.01

Kemp, A. I. S., Hawkesworth, C. J., Foster, G. L., Paterson, B. A., Woodhead, J. D., Hergt, J. M., et al. (2007). Magmatic and crustal differentiation history of granitic rocks from Hf-O isotopes in zircon. *Science*, *315*(5814), 980–983. https://doi.org/10.1126/science.1136154

Kowalski, P. M., & Wunder, B. (2018). Boron isotope fractionation among vapor–liquids–solids–melts: Experiments and atomistic modeling. *Boron isotopes: The fifth element* (pp. 33–69).

Leake, B. E., Woolley, A. R., Arps, C. E., Birch, W. D., Gilbert, M. C., Grice, J. D., et al. (1997). Nomenclature of amphiboles; report of the Subcommittee on Amphiboles of the International Mineralogical Association Commission on new minerals and mineral names. *Mineralogical Magazine*, *61*(405), 295–310. https://doi.org/10.1180/minmag.1997.061.405.13

Li, M. J., Zeng, Y. C., Tiepolo, M., Farina, F., Xu, J. F., Huang, F., et al. (2023). Grain-scale zircon Hf isotope heterogeneity inherited from sediment-metasomatized mantle: Geochemical and Nd-Hf-Pb-O isotopic constraints on Early Cretaceous intrusions in central Lhasa Block, Tibetan Plateau. *American Mineralogist*, *108*(9), 1692–1707. https://doi.org/10.2138/am-2022-8508

Li, M. J., Zeng, Y. C., Tiepolo, M., Xu, J. F., Cannaò, E., Forni, F., & Huang, F. (2024). The capability of amphibole in tracing the physico-chemical processes of magma mixing [Dataset]. *OSF*. http://osf.io/crmwz

Li, X., Liu, X., Liu, Y., Su, L., Sun, W., Huang, H., & Yi, K. (2015). Accuracy of LA-ICPMS zircon U-Pb age determination: An inter-laboratory comparison. *Science China Earth Sciences*, *58*(10), 1722–1730. https://doi.org/10.1007/s11430-015-5110-x

Loucks, R. R., Fiorentini, M. L., & Henríquez, G. J. (2020). New magmatic oxybarometer using trace elements in zircon. *Journal of Petrology*, *61*(3), egaa034. https://doi.org/10.1093/petrology/egaa034

Marschall, H. R., Wanless, V. D., Shimizu, N., Von Strandmann, P. A. P., Elliott, T., & Monteleone, B. D. (2017). The boron and lithium isotopic composition of mid-ocean ridge basalts and the mantle. *Geochimica et Cosmochimica Acta*, *207*, 102–138. https://doi.org/10.1016/j.gca.2017.03.028

Palmer, M. R., & Swihart, G. H. (1996). Boron isotope geochemistry; an overview. *Reviews in Mineralogy and Geochemistry*, *33*(1), 709–744.

Ridolfi, F., Renzulli, A., & Puerini, M. (2010). Stability and chemical equilibrium of amphibole in calc-alkaline magmas: An overview, new thermobarometric formulations and application to subduction-related volcanoes. *Contributions to Mineralogy and Petrology*, *160*(1), 45–66. https://doi.org/10.1007/s00410-009-0465-7

Schmidt, M. W. (1992). Amphibole composition in tonalite as a function of pressure: An experimental calibration of the Al-in-hornblende barometer. *Contributions to Mineralogy and Petrology*, *110*(2–3), 304–310. https://doi.org/10.1007/bf00310745

Smith, D. J. (2014). Clinopyroxene precursors to amphibole sponge in arc crust. *Nature Communications*, *5*(1), 4329. https://doi.org/10.1038/ncomms5329

Spencer, C. J., Cawood, P. A., Hawkesworth, C. J., Raub, T. D., Prave, A. R., & Roberts, N. M. (2014). Proterozoic onset of crustal reworking and collisional tectonics: Reappraisal of the zircon oxygen isotope record. *Geology*, *42*(5), 451–454. https://doi.org/10.1130/g35363.1

Tiepolo, M., Oberti, R., Zanetti, A., Vannucci, R., & Foley, S. F. (2007). Trace-element partitioning between amphibole and silicate melt. *Reviews in Mineralogy and Geochemistry*, *67*(1), 417–452. https://doi.org/10.2138/rmg.2007.67.11

Tonarini, S., Leeman, W. P., & Leat, P. T. (2011). Subduction erosion of forearc mantle wedge implicated in the genesis of the South Sandwich Island (SSI) arc: Evidence from boron isotope systematics. *Earth and Planetary Science Letters*, *301*(1–2), 275–284. https://doi.org/10.1016/j.epsl.2010.11.008

Valley, J. W., Lackey, J. S., Cavosie, A. J., Clechenko, C. C., Spicuzza, M. J., Basei, M. A. S., et al. (2005). 4.4 billion years of crustal maturation: Oxygen isotope ratios of magmatic zircon. *Contributions to Mineralogy and Petrology*, *150*(6), 561–580. https://doi.org/10.1007/s00410-005-0025-8

Wang, D., Romer, R. L., Guo, J. H., & Glodny, J. (2020). Li and B isotopic fingerprint of Archean subduction. *Geochimica et Cosmochimica Acta*, *268*, 446–466. https://doi.org/10.1016/j.gca.2019.10.021

Wei, Y. F., Xiao, Q. R., Luo, W., Qiu, C. Y., Deng, Z. J., Zhao, Z. Q., & Lin, M. Y. (2018). Zircon U-Pb age, geochemistry and geological significance of high Nb-Ta acid volcanic rocks from Meisu Formation, Bieruo-Zecuo area, Gangdise belt. *Geological Bulletin of China*, *37*(6), 1015–1025.

Zeng, Y. C., Xu, J. F., Huang, F., Li, M. J., & Chen, Q. (2020). Generation of the 105–100 Ma Dagze volcanic rocks in the north Lhasa Block by lower crustal melting at different temperature and depth: Implications for tectonic transition. *Geological Society of America Bulletin*, *132*(5–6), 1257–1272. https://doi.org/10.1130/b35306.1

Zhu, D. C., Zhao, Z. D., Niu, Y., Mo, X. X., Chung, S. L., Hou, Z. Q., et al. (2011). The Lhasa Block: Record of a microcontinent and its histories of drift and growth. *Earth and Planetary Science Letters*, *301*(1–2), 241–255. https://doi.org/10.1016/j.epsl.2010.11.005

References From the Supporting Information

Anderson, D. L. (1989). *Theory of the Earth* (p. 366). Blackwell Scientific.

Bao, Z. A., Zong, C. L., Fang, L. R., Yuan, H. L., Chen, K. Y., & Dai, M. N. (2018). Determination of Hf–Sr–Nd isotopic ratios by MC-ICP-MS using rapid acid digestion after flux-free fusion in geological materials. *Acta Geochimica*, *37*(2), 244–256. https://doi.org/10.1007/s11631-017-0207-x

Belousova, E. A., Griffin, W. L., O'Reilly, S. Y., & Fisher, N. L. (2002). Igneous zircon: Trace element composition as an indicator of source rock type. *Contributions to Mineralogy and Petrology*, *143*(5), 602–622. https://doi.org/10.1007/s00410-002-0364-7

Bindeman, I. N., Davis, A. M., & Drake, M. J. (1998). Ion microprobe study of plagioclase-basalt partition experiments at natural concentration levels of trace elements. *Geochimica et Cosmochimica Acta*, *62*(7), 1175–1193. https://doi.org/10.1016/s0016-7037(98)00047-7

Blichert-Toft, J., & Albarède, F. (1997). The Lu–Hf geochemistry of chondrites and the evolution of the mantle–crust system. *Earth and Planetary Science Letters*, *148*, 24–258.

Catanzaro, E. J., Champion, C. E., Garner, E. L., Marinenko, G., Sappenfield, K. M., & Shields, W. R. (1970). *Boric acid: Isotopic and assay standard reference materials* (Vol. 260, pp. 1–70). National Bureau of Standards, Institute for Materials Research.

Elhlou, S., Belousova, E., Griffin, W. L., Pearson, N. J., & O'Reilly, S. Y. (2006). Trace element and isotopic composition of GJ-red zircon standard by laser ablation. *Geochimica et Cosmochimica Acta*, *70*(18), 158. https://doi.org/10.1016/j.gca.2006.06.1383

He, M., Xia, X., Huang, X., Ma, J., Zou, J., Yang, Q., et al. (2020). Rapid determination of the original boron isotopic composition from altered basaltic glass by: In situ secondary ion mass spectrometry. *Journal of Analytical Atomic Spectrometry*, *35*(2), 238–245. https://doi.org/10.1039/c9ja00374f

Horstwood, M. S., Košler, J., Gehrels, G., Jackson, S. E., McLean, N. M., Paton, C., et al. (2016). Community-derived standards for LA-ICP-MS U-(Th-) Pb geochronology–Uncertainty propagation, age interpretation and data reporting. *Geostandards and Geoanalytical Research*, *40*(3), 311–332. https://doi.org/10.1111/j.1751-908x.2016.00379.x

Ickert, R. B., Hiess, J., Williams, I. S., Holden, P., Ireland, T. R., Lanc, P., et al. (2008). Determining high precision, in situ, oxygen isotope ratios with a SHRIMP II: Analyses of MPI-DING silicate-glass reference materials and zircon from contrasting granites. *Chemical Geology*, *257*(1–2), 114–128. https://doi.org/10.1016/j.chemgeo.2008.08.024

Jackson, S. E., Pearson, N. J., Griffin, W. L., & Belousova, E. A. (2004). The application of laser ablation-inductively coupled plasma-mass spectrometry to in situ U-Pb zircon geochronology. *Chemical Geology*, *211*(1–2), 47–69. https://doi.org/10.1016/j.chemgeo.2004.06.017

Jochum, K. P., Wilson, S. A., Abouchami, W., Amini, M., Chmeleff, J., Eisenhauer, A., et al. (2011). GSD-1G and MPI-DING reference glasses for in situ and bulk isotopic determination. *Geostandards and Geoanalytical Research*, *35*(2), 193–226. https://doi.org/10.1111/j.1751-908x.2010.00114.x

Li, X. H., Long, W. G., Li, Q. L., Liu, Y., Zheng, Y. F., Yang, Y. H., et al. (2010). Penglai zircon megacrysts: A potential new working reference material for microbeam determination of Hf–O isotopes and U–Pb age. *Geostandards and Geoanalytical Research*, *34*(2), 117–134. https://doi.org/10.1111/j.1751-908x.2010.00036.x

Li, X. H., Tang, G. Q., Gong, B., Yang, Y. H., Hou, K. J., Hu, Z. C., et al. (2013). Qinghu zircon: A working reference for microbeam analysis of U-Pb age and Hf and O isotopes. *Chinese Science Bulletin*, *58*(36), 4647–4654. https://doi.org/10.1007/s11434-013-5932-x

Liu, Y. S., Hu, Z. C., Gao, S., Günther, D., Xu, J., Gao, C. G., & Chen, H. L. (2008). In situ analysis of major and trace elements of anhydrous minerals by LA-ICP-MS without applying an internal standard. *Chemical Geology*, *257*(1–2), 34–43. https://doi.org/10.1016/j.chemgeo.2008.08.004

Lugli, F., Weber, M., Giovanardi, T., Arrighi, S., Bortolini, E., Figus, C., et al. (2020). Fast offline data reduction of laser ablation MC-ICP-MS Sr isotope measurements via an interactive Excel-based spreadsheet 'SrDR'. *Journal of Analytical Atomic Spectrometry*, *35*(5), 852–862. https://doi.org/10.1039/c9ja00424f

Sláma, J., Košler, J., Condon, D. J., Crowley, J. L., Gerdes, A., Hanchar, J. M., et al. (2008). Plešovice zircon—A new natural reference material for U–Pb and Hf isotopic microanalysis. *Chemical Geology*, *249*(1–2), 1–35. https://doi.org/10.1016/j.chemgeo.2007.11.005

Soderlund, U., Patchett, P. J., Vervoort, J. D., & Isachsen, C. E. (2004). The ^{176}Lu decay constant determined by Lu–Hf and U–Pb isotope systematics of Precambrian mafic intrusions. *Earth and Planetary Science Letters*, *219*(3–4), 311–324. https://doi.org/10.1016/s0012-821x(04)00012-3

Spencer, C. J., Kirkland, C. L., Roberts, N. M. W., Evans, N. J., & Liebmann, J. (2020). Strategies towards robust interpretations of in situ zircon Lu–Hf isotope analyses. *Geoscience Frontiers*, *11*(3), 843–853. https://doi.org/10.1016/j.gsf.2019.09.004

Sun, S., & McDonough, W. F. (1989). Chemical and isotopic systematics of oceanic basalts: Implications for mantle composition and processes. In A. D. Saunders & M. J. Norry (Eds.), *Magmatism in the Ocean Basins* (Vol. 42, pp. 313–345). Geological Society, London, Special Publication. https://doi.org/10.1144/gsl.sp.1989.042.01.19

Tribuzio, R., Thirlwall, M. F., & Messiga, B. (1999). Petrology, mineral and isotope geochemistry of the Sondalo gabbroic complex (Central Alps, Northern Italy): Implications for the origin of post-Variscan magmatism. *Contributions to Mineralogy and Petrology*, *136*(1–2), 48–62. https://doi.org/10.1007/s004100050523

Vannucci, R., Bottazzi, P., Wulff-Pedersen, E., & Neumann, E. R. (1998). Partitioning of REE, Y, Sr, Zr and Ti between clinopyroxene and silicate melts in the mantle under La Palma (Canary Islands): Implications for the nature of the metasomatic agents. *Earth and Planetary Science Letters*, *158*(1–2), 39–51. https://doi.org/10.1016/s0012-821x(98)00040-5

Weis, D., Kieffer, B., Maerschalk, C., Barling, J., de Jong, J., Williams, G. A., et al. (2006). High-precision isotopic characterization of USGS reference materials by TIMS and MC-ICP-MS. *Geochemistry, Geophysics, Geosystems*, *7*(8), Q08006. https://doi.org/10.1029/2006gc001283

Wu, F. Y., Yang, Y. H., Xie, L. W., Yang, J. H., & Xu, P. (2006). Hf isotopic compositions of the standard zircons and baddeleyites used in U–Pb geochronology. *Chemical Geology*, *234*(1–2), 105–126. https://doi.org/10.1016/j.chemgeo.2006.05.003

Zhou, X., Zheng, J. P., Xiong, Q., Yang, J. S., Wu, Y. B., Zhao, J. H., et al. (2017). Early Mesozoic deep-crust reworking beneath the central Lhasa terrane (South Tibet): Evidence from intermediate gneiss xenoliths in granites. *Lithos*, *274*, 225–239. https://doi.org/10.1016/j.lithos.2016.12.035

Zhu, D. C., Zhao, Z. D., Niu, Y., Dilek, Y., Hou, Z. Q., & Mo, X. X. (2013). The origin and pre-Cenozoic evolution of the Tibetan Plateau. *Gondwana Research*, *23*(4), 1429–1454. https://doi.org/10.1016/j.gr.2012.02.002